

USING SUPPORT VECTOR MACHINE TO IDENTIFY LAND COVER CHANGE DURING COVID-19 PANDEMIC IN KOMODO NATIONAL PARK, INDONESIA

Laode Muhammad Golok Jaya^{1*}, Rizal Adi Saputra¹, Sitti Hairani Idrus²

¹Department of Informatics Engineering, Halu Oleo University, Jl. HEA Mokodompit Kampus Hijau UHO Bumi Tridharma Anduonohu, Kendari, Sulawesi Tenggara (93232), Indonesia.

²Department of Business Administration, Halu Oleo University, Jl. HEA Mokodompit Kampus Hijau UHO Bumi Tridharma Anduonohu, Kendari, Sulawesi Tenggara (93232), Indonesia.

*Corresponding author: laodemgj@uho.ac.id

Received: March 27th, 2022 / Accepted: August 8th, 2022 / Published: October 01st, 2022

<https://DOI-10.24057/2071-9388-2022-030>

ABSTRACT. The Covid-19 pandemic affects many areas of life, including the tourism sector. Furthermore, it significantly reduced the number of people visiting tourist destinations, and the reduction has helped to improve the environment in the National Park. Therefore, this study aims to present a satellite image classification method using Support Vector Machine to identify changes in the vegetation area of Komodo National Park. The satellite image used was created with Google Earth Pro with a resolution of 1920 x 1280 pixels using data collected in 2019 and 2020 before and during the pandemic. This study focuses on six tourist destinations in Komodo National Park: Loh Liang, Loh Buaya, Padar Island, Kanawa Island, Pink Beach, and Loh Sebita. The image was pre-processed using radiometric calibration, atmospheric correction, and contrast enhancement. The results of the pre-processing showed that segmentation will be performed to distinguish the area between one class and another. Furthermore, the image will be classified into five classes using the Support Vector Machine, including Soil, Vegetation, Built-Up Area, Deep Water, and Shallow Water. The measurement of the area of vegetation from 2019 and 2020 using Otsu's thresholding showed environmental changes. Meanwhile, environmental improvements occurred in seven areas in the vegetation area category, with a 31.86% rise from 2019 to 2020. The increase in the area of green areas in the Komodo National Park all because tourist restriction and there is no climate fluctuations during the time of study.

KEYWORDS: Vegetation Area Change, Environmental Recovery, Machine Learning, Support Vector Machine, Komodo National Park

CITATION: Jaya L.M.G., Saputra R.A., Idrus S.H. (2022). Using Support Vector Machine To Identify Land Cover Change During Covid-19 Pandemic In Komodo National Park, Indonesia. *Geography, Environment, Sustainability*. 3(15), 70-79

<https://DOI-10.24057/2071-9388-2022-030>

Conflict of interests: The authors reported no potential conflict of interest.

INTRODUCTION

The coronavirus (Covid-19) first hit the world in December 2019 in Wuhan, China. It then continued to spread around the world, with more than 236 million confirmed cases and 4.8 million deaths in 223 countries (WHO 2021). With around 4.2 million confirmed cases by the end of September 2021, Indonesia is one of the countries with the most infections in the world (Worldometer 2021). According to WHO, the group of cases affected have mild to severe respiratory symptoms and will recover without additional treatment. However, with limited healthcare facilities, many cases end in death. The Ministry of Health reported 141.743 overall death cases by the end of September 2021 (Health Ministry of Indonesia 2021).

The Government has taken several measures in response to the Covid-19 pandemic, including travel restrictions. On 31 March, the Ministry of Law and Human Rights issued Regulation Number 11 of 2020 Concerning Temporary Prohibition for Foreigners to Enter Indonesia (Regulation 11/2020). Currently, Covid-19 Task Force has continued to temporarily ban the entry of all foreign

visitors except for people with work permits, business visas, permanent residence, diplomatic visas, as well as those who traveling under special corridor arrangements (Medina 2021). For domestic travelers, different guidelines have been introduced to help to contain the Covid-19 virus. It started with the cancellation of all international and domestic commercial flights from April 24th, 2020, until May 31st, 2020. However, Indonesian can travel under some circumstances such as negatives PCR Test results and evidence of being vaccinated (minimum one doses) (Kemenlu RI 2021).

Travel bans, strict travel rules, and Covid-19 itself have all impacted the domestic and global tourism sectors at the national level. Badan Pusat Statistics (BPS), the statistical center of Indonesia, reported that the number of international tourists fell 47.02% from April to December 2020 compared to the first quarter of 2020. The decline continued until 2021 since only 937,747 visited in July 2021, and the number dropped by 71.42% from the same period last year (BP, 2021a). This outbreak has affected all tourist destinations, including Komodo National Park (Veyadi Purba et al. 2021).

Komodo National Park is located between the islands of Sumbawa and Flores in the middle of the Indonesian archipelago. The Park was founded in 1980 with the primary objective of protecting the endangered Komodo dragon (*Varanus komodoensis*) and its environment. However, it has evolved through time to include the protection of its entire terrestrial and marine diversities (UNESCO 2020). In 1986, the Park was designated as a World Heritage Site and a Man and Biosphere Reserve by UNESCO, emphasizing its biological importance.

Komodo National Park is home to several other significant terrestrial species, including the orange-footed scrub fowl, a unique rat, and the Timor deer. The rising demand for forest cover and water resources as more tourists visit Komodo National Park poses a threat to terrestrial biodiversity (Ariefandy et al. 2021). During the incidence of Covid-19 in 2020, only 51618 tourists visited the park. The number fell drastically compared to the previous year which reached 221708 people (BPS 2021b). In addition, to influence the decline in foreign exchange from the tourism sector, there is a positive impact from the decrease of tourist number, such as the improvement of the vegetation and ecosystem of the Komodo National Park.

Several studies related to area changes in national parks have also been carried out by several researchers, such as the Oni Gambari reserve, Ibadan, Nigeria (Khadijat et al. 2021); Lake Malombe, Southern Malawi (Makwinja et al. 2021); and Sikkim Himalayas, India (Mishra et al., 2020). According to the studies, a satellite image classification can determine the change of area on some period of time. Although in this study only using two (2) years data image, but some preprocessing method and a detailed object classification using Support Vector Machine could bring a good result to this study (Talukdar et al. 2020). By using SVM, it is expected to be able to separate vegetated and non-

vegetated areas and be able to prove the hypothesis that there is an additional vegetation area in Komodo National Park during the COVID-19 pandemic.

MATERIAL AND METHODS

The primary focus is to offer a reliable satellite classification system using SVM method that uses image pre-processing, segmentation, classification phases, and land cover and use change analyses. This study will classified the area of Komodo National Park into vegetation or non vegetation area based on image satellite. The processed image can be used to acquire information on the total area of vegetation in Komodo National Park during pandemic Covid-19. The stages of this research include data acquisition using images from google earth followed by pre-processing using radiometric calibration and atmospheric correction which then improves contrast by means of histogram equalization. The pre-processed image will then be subjected to an object detection process to separate the vegetation and non-vegetation objects. From objects that have been detected, MultiSVM will then be used to classify objects into previously prepared labels. The final stage of this research is to calculate the area of vegetation and non-vegetation based on images in different years using LULC digital image processing with several stages to obtain the area of vegetation before and after the pandemic. Figure 1 shows framework from this study.

Study Area

Komodo National Park has three large islands: Komodo, Rinca, and Padar, as well as several smaller islands, totaling 1817 km² (marine and land), with proposed extensions that can bring the total surface area up to 2321 km²

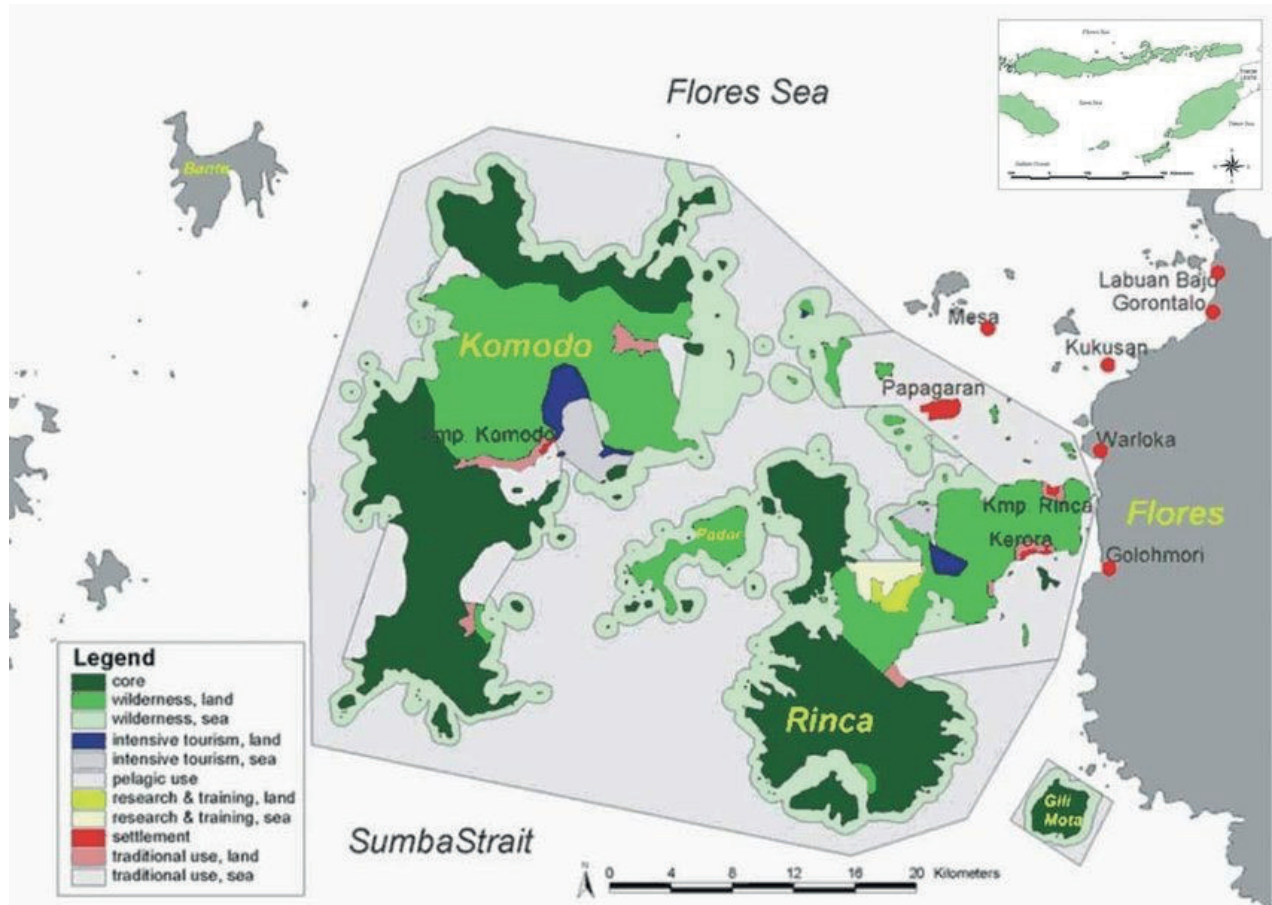


Fig. 1. Zoning Komodo National Park Area
(www.komodonationalpark.org, n.d.)

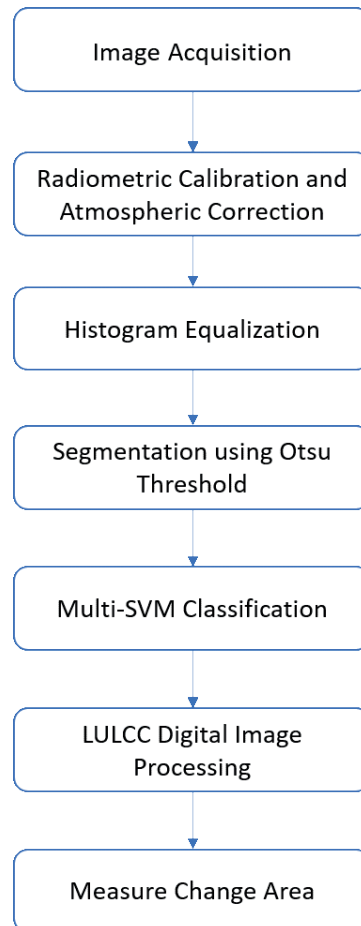


Fig. 2. Framework of research

(Komodo National Park 2017). There are presently almost 4,000 people living within the park spread out over four settlements (Komodo, Rinca, Kerora, and Papa Garang) and only Komodo and Papa Garang have a habitant. All villages existed before 1980 when the area was declared a national park. At the 2020 Census, Komodo Village had 1,845 inhabitants and Papagaran Village had 1,493 inhabitants. The total population currently living in the park is 3,338 people with 16,816 people live in the area immediately surrounding the park (Harum 2021). This study focuses on six tourist destinations in Komodo National Park: Loh Liang, Loh Buaya, Padar Island, Kanawa Island, Pink Beach, and Loh Sebita. In the focuses study area there are none villagers building, there is only office building for entrance and some bungalow.

Data Used

The data downloaded using Google Earth Pro with the original size is 1920 x 1080 pixels and a resolution of 96 dpi. Furthermore, there are 22 images from 11 tourist spot locations in Komodo National Park, and the tourist spots are used by following the map in Figure 1. The intensive tourism land region include Loh Buaya, Loh Liang, Loh Sebita, Pink Beach, Kanawa Island, and Padar Island. In addition, the satellite image used were acquired in 2019 and 2020 in the same season and taken in the morning at 08.00 (GMT+8) to compare the area of vegetation change during the Covid-19 pandemic. Table 1 showed the precise parameters and the acquired data.

Preprocessing

Image pre-processing is also known as a satellite image data pre-analysis, and it is used to enhance digital geospatial

information into a presentation that is more meaningful to users. Furthermore, it offers quantifiable information about an item and can solve issues. In pre-processing, the image captured by the sensor will be normalized to process the image at the feature separation stage. The quality of the features produced in the separation process is highly dependent on the results of pre-processing. In this study, radiometric calibration and atmospheric correction were used for image preprocessing (Talukdar et al. 2020).

Radiometric Calibration

Radiometric calibration, also known as radiometric correction converts raw digital image data from satellites or aerial sensors to a regularly occurring scale based on verified reflectance measurements from ground surface objects. When working with satellite image data, the first step is to conduct radiometric calibration. The primary goal is to transform image data recorded as a Digital Number (DN) into radiance and/or reflectance, as well as brightness temperature for Thermal Infrared channels (Thome et al. 1997). Furthermore, Score Spectral radians are used for processing related to the surface temperature. The value of reflectance is the ratio of the reflected energy (and received by the sensor) with the object. The unit does not exist (dimensionless) since reflectance is widely used for processing indexes. The vegetation index, for example, produces the best results when processed using reflectance measurements. Meanwhile, atmospheric correction should be conducted which corrects the sun position, recording angle, and topography of the area to obtain a good reflectance value.

Table 1. Satellite Image of Tourism Area in Komodo National Park

No	Name	Picture 2019	Picture 2020	Source Data
1	Loh Liang			Google Earth Pro application was used to get the data. The images for 2019 were taken on December 19 th , while the images for 2020 were taken on December 16 th , 2020. Both photos were shot around 8 a.m.
2	Kanawa Island			
3	Loh Buaya			
4	Pink Beach			
5	Padar Island Entrance			
6	Padar Island Tracking Area			
7	Loh Sebita			

Convert Digital Number (DN) to Top of Atmosphere (TOA) Radiance

To obtain the spectral radian value, pixel rescaling should be conducted using the same value listed in the metadata (Jaelani 2015). The equation used is:

$$L_{\lambda} = M_L Q_{cal} + A_L \tag{1}$$

with

- L_{λ} = TOA spectral radiance ($watss/(m^2 * srad * \mu m)$)
- M_L = A multiplicative rescaling factor for each band from metadata
- A_L = A band-specific additive rescaling factor from the metadata
- Q_{cal} = Quantized and calibrated standard product pixel values (DN)

Convert Digital Number (DN) to Top of Atmosphere (TOA) Reflectance

For the thermal band, the correction level is only at conversion into spectral radian values since it is not a reflecting band but thermal infrared energy (Jaelani 2014). The correction on Landsat-8 does not use the value spectral

radian (L_{λ}) but rescaling pixels value (Q_{cal}). Reflectance correction was obtained by the equation:

$$\rho_{\lambda} = M_{\rho} Q_{cal} + A_{\rho} \tag{2}$$

with

- ρ_{λ} = TOA planetary reflectance, without any adjustment for the angle of the sun It should be noted that ρ_{λ} does not include an adjustment for the sun angle
- M_{ρ} = A multiplicative rescaling factor for each band from metadata
- A_{ρ} = A band-specific additive rescaling factor from the metadata
- Q_{cal} = Quantized and calibrated standard product pixel values (DN)

Atmospheric Correction

This adjustment was conducted by considering a variety of atmospheric characteristics, such as seasonal variables and environmental circumstances at the picture recording site (e.g., tropical, sub-tropical, etc.). The advantages are in the ability to correct atmospheric disturbances such as haze, smoke, and others (Yuniar 2018). The primary goal is to transform sensor data (at sensor reflectance or Top of

Atmosphere reflectance) into surface reflectance (Bottom of Atmosphere reflectance) using the basic schema correction atmosphere algorithm as follows:

$$\rho_{toa}(\lambda) = \rho_r(\lambda) + [\rho_a(\lambda) + \rho_{ra}(\lambda)] + t(\lambda)\rho_w(\lambda) \quad (3)$$

with

$\rho_{toa}(\lambda)$ = satellite sensor captured reflectance

$\rho_r(\lambda)$ = Rayleigh scattering reflectance

$\rho_a(\lambda) + \rho_{ra}(\lambda)$ = total reflectance due to aerosol scattering, as well as the interplay between Rayleigh and aerosol scattering

$t(\lambda)$ = diffuse transmittances of atmospheric column

$\rho_w(\lambda)$ = water leaving reflectance (surface reflectance, Bottom of Atmosphere reflectance)

Contrast Enhancement Using Histogram Equalization

Histogram Equalization is a computer-assisted image processing approach for enhancing picture contrast (Rao 2020). This is accomplished by spreading out some of the most frequent intensity values, i.e., broadening the intensity range of the image. When such usable data is processed by near contrast values, this method improves the global contrast (X. Wu et al. 2017), and this permits areas with poor local contrast to gain more contrast. Furthermore, the method enhances the general contrast of numerous pictures, specifically when the image is represented by a narrow range of intensity values. By making use of the varying intensities evenly, it may be better dispersed on the histogram with this change, and this enables areas with poor local contrast to gain more contrast. Histogram equalization is conducted by efficiently distributing the highly dense intensity values required to reduce image contrast (Voronin 2019). The Bi-Histogram Equalization was used to spread the pixel of the satellite image and also to differentiate between various colors of objects.

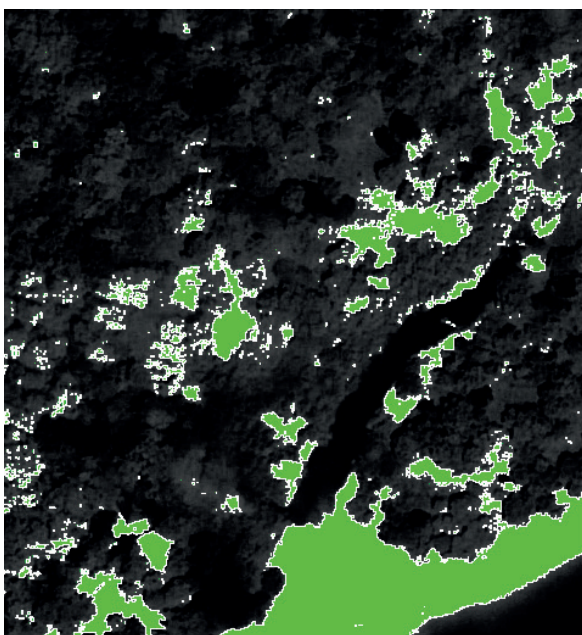
Object Detection

Object detection in digital image processing is a process used to determine the existence of certain objects in a digital image (Naiemi et al. 2021). The detection process can be conducted by various methods which generally read the features of all objects in the input image. The features of the object in the input images will be compared to the reference

or template's features. Meanwhile, the comparison results can be used to determine whether an object is detected as the intended template or not. Image segmentation was used in this study because it provides pixel-by-pixel detail of an object, making it distinct from object classification and detection. The image is split into homogenous object primitives during image segmentation, and it is a preparatory step in object-oriented image classification. Multi-resolution segmentation was used to segment the study area, which decreases the average heterogeneity of image objects at a given resolution. The scale parameter is an arbitrary integer that determines the amount of heterogeneity tolerated in the image objects. A higher scale value results in bigger things, and vice versa. In addition, it is good when the image items are smaller than the real things since larger objects are more prone to errors. The three factors that can characterize an object's heterogeneity are color, smoothness, and compactness (C. F. Wu et al. 2016).

The compactness of an item is defined by its perimeter and the boundary of the object's enclosing box. Meanwhile, the smoothness is determined by its boundary and the number of pixels within it, and these criteria describe the object's shape. The shape and color together define the object's homogeneity, and manual analysis is widely regarded as the most accurate method. The diversity of values for each variable and the combinations were tested to analyze the affected segmentation performance (Wang et al. 2021). The variables of the multi-resolution segmentation process were determined through trial and error to ensure the final segmentation matched the graphical illustration. Initially, a correlation analysis was performed to decrease the redundancy of the bands included in the segmentation. Due to the general high correlations among bands, this study performs multiple segmentation by using the Otsu Thresholding method to gain each feature required. It is used to recognize "large" items such as land, water, forests, building, etc. The Otsu technique divides the histogram of a gray level image into two regions without the need for a threshold value to be entered by the user (Otsu 1979). It employs discriminant analysis, which entails identifying a variable that can differentiate between two or more groups (Saputra 2021). The thresholds value that should find examples expressed by k which value ranges from 1-255 since the value of k chosen is the maximum of the equation by using formula:

$$\sigma_B^2(k^*) = \max_{1 \leq k \leq L} \sigma_B^2(k) \quad (4)$$



(a)



(b)

Fig. 3. (a) Segmentation using Otsu Threshold (b) Masking area with Original Image

For a better object classification, original image was divided into 60 smaller of the as shown in figure 3. Figure 3 showed that soil and building area was the first segmentation to be distinguished from forest and waters. The second segmentation will be used to differentiate between soil and structure, as well as forest and water. A total of 5 classes were extracted from this study, and they are soil, forests, buildings, deep water, and shallow water.

Classification Using Support Vector Machine (SVM)

SVM is a supervised classification method used to categorize items by establishing a boundary between them, and binary SVM is not practical for tasks with many categories (López-Serrano et al. 2016). Multiple continuous and categorical variables, as well as linear and non-linear samples in various class memberships, can also be supported by SVM (Shih et al. 2019). Unlike the neural network approach, which seeks a separating hyperplane across classes, this classification obtains the optimal hyperplane in the input space. It was created as a linear classifier but was later improved to cope with non-linear problems by incorporating the kernel notion into a high-dimensional workspace. Furthermore, it identifies the optimum hyperplane separator between two classes by maximizing the margin between each class's nearest points (Anantrasirichai et al. 2018).

Multiclass SVM includes five different classes of soil, vegetation, built-up area, shallow water, and deep water. Support vectors are the training or bordering samples that define the margin or hyper-plane of SVM. This study uses $n(n-1)$ classifiers to distinguish between classes, and the final decisions are considered. Finally, the areas are categorized according to the maximum-voting policy, and all the distinct classes are processed at the same time by calculating the equation below. The slack variable is sv , the bias is b , and both appear to be normal to the hyperplane., $i = 1,2, \dots r$ is the number of classes, and y is the number of training samples. The following equation is used to make a final decision:

$$decn = \max \tag{5}$$

$$y(wyp\beta(xi) + by) \tag{6}$$

this study's kernel function was a linear function with a formula:

$$k(x, y) = x, y \tag{7}$$

Where x and y are two data pairs of all training sections. In this method, each pair of classes is subjected to all the classifiers. Consider an object that should be classified into

one of three categories (say x,y,z), and this is achieved by applying all the classifiers to an image. When a classifier defines an item as belonging to class x , the value is increased by one, and the maximum votes are used to make the final classification decision (Farda 2017). This method gives accurate results in a fair amount of time (Pelletier et al. 2017).

The second binary image was created by combining the land (rock, vegetation) and water characteristics from the coastal-surface categorization map. Meanwhile, the second coastline was recovered from the improved second binary picture by choosing the boundary between the detected land and water features. Then morphological filtering was used to refine the border between the land and water features in the second binary image. The checkpoints were used to assess the accuracy of both produced shorelines to choose the best technique for the shoreline mapping assignment. Figure 4 showed the result of sample classification using SVM on Loh Liang and Kanawa Island.

Land Use and Land Cover Change (LULCC) Analysis

Land-use change refers to alterations in how a single piece of land is exploited or maintained by people. Meanwhile, land-cover change is an alteration in the continuous characteristics of the land, such as the type of plant and soil quality (Majumdar 2020). This involves the natural landscape being altered because of population expansion (Verma et al. 2020). It should be noted that this alteration can cause a slew of local and global effects, including biodiversity loss and its implications for human health, as well as ecosystem damage (Patel et al. 2019). In recent studies on sustainable development, planning, and management, monitoring and mapping LULCC has become increasingly essential (Mishra et al. 2020). In this study, LULCC analysis used the following digital image processing.

Color Threshold

The Color Threshold is used to eliminate picture portions within a certain color range. This method is useful for detecting items with constant color values (Al Mamun et al. 2021), and the interface showed the histograms in red, green, and blue. The histogram contains the value and number of each pixel (0-255 and 0-image size) with that color value. It is used to remove pixels with the values from the picture, leaving only the desired object visible. All the green colors from vegetation were set to white pixels, which were disregarded by the histogram in the image.

Table 2. Description of the land use/land cover LULLC classes identified

Class Name	Class Description	Clas Description Example
Soil Area	Area without vegetation	
Vegetation Area	Area covered by trees, forest, sparse. etc.	
Built-Up Areas	This are include all of structure made by human example building, dock, ship,etc	
Deep Water	Area covered by water	
Shallow Water	Area covered by water but with the turquoise blue color (beach)	

This enables images to have a useful histogram even when dark or bright. Furthermore, these values can be re-added, but they have no impact on the threshold operation.

Convert Image RGB to Grayscale 8-bit

When converting a picture from RGB to 8-bit grayscale, down-sampling occurs when 24-bit information is squeezed into the range. The simplest method is to use a straight translation that averages the red, green, and blue values for each pixel. To estimate the human luminance viewpoint, a conversion with color-specific weights is appropriate to estimate the human luminance viewpoint (Putra 2010). Therefore, this study aims to RGB's image to 8-bit grayscale using formula:

$$Grayscale = 0.299R + 0.587G + 0.114B \tag{8}$$

When the RGB image is transformed into grayscale, the value of each pixel is reduced from three to one. This defines the regional boundaries between one area class and another. In this study, the vegetation area will remain white, while others will be gray to black.

Invert to LUT Threshold

LUT is an acronym for Look-Up Table, and it converts one color range in an image to another. For 8-bit pictures, the value (v) of each table item is substituted with 255-v (Lee et al. 2018), and the pixels with a value of zero are white.



- Legend**
- Vegetation
 - Soil
 - Build up area
 - Deep water
 - Shallow water

Fig. 4. Classification using SVM on Loh Liang and Kanawa Island

Meanwhile, the pixels with a value of 255 are black when using inverted LUTs. The vegetations used were white and were inverted into black and other areas were inverted to white.

Measure Area

In the next step, the area of vegetation is measured by counting all pixels that represent the area. Black pixels were measured from an inverted threshold image of a region in Komodo National Park for this investigation. The area that has more vegetation was darker than those with less vegetation. Figure 5 showed all the digital image processing used to analyze the land cover change of Komodo National Park.

Classification results using SVM are then calculated using a confusion matrix for accuracy assessment of LULCC classification of the years 2019 and 2020. The result of confusion matrix shown in Table 3 and Table 4. With Kappa coefficient of 90% and 88% in 2019 and 2020, the confusion matrix produced overall very good accuracies for the five classification points and the defined LULCC classes. Both class-specific user accuracies and producer's accuracies were at least 81%, suggesting that a considerable percentage of pixels were correctly classified.

RESULTS AND DISCUSSION

The areas measure in seven tourist sites of Komodo National Park discovered a significant change of land cover specifically the vegetation that increased between

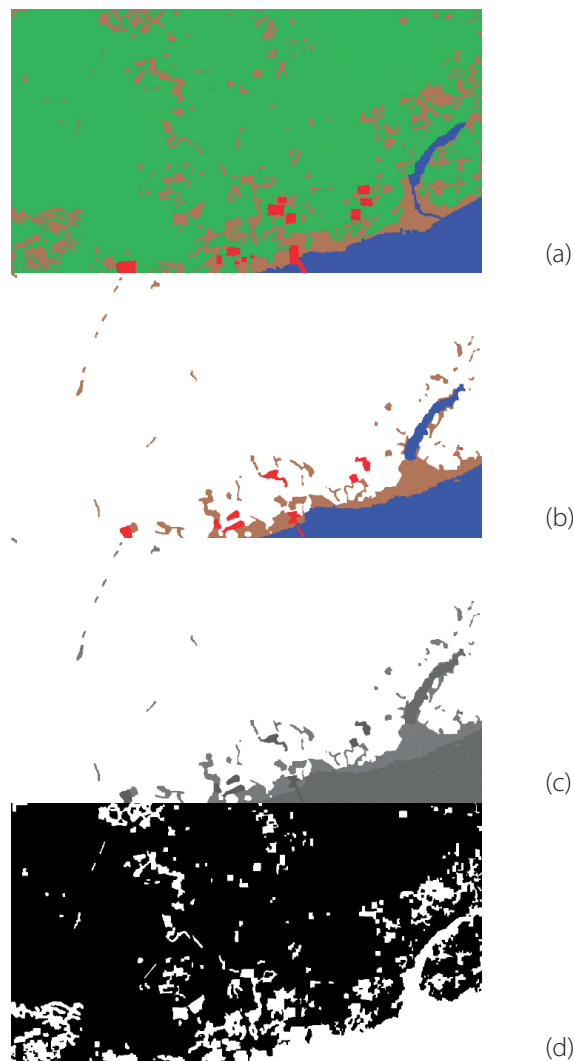


Fig. 5. (a) Original RGB Image, (b) Colour Threshold, (c) Grayscale Image 8-bit, and (d) Inverted LUT Image

Table 3. Confusion matrix of classification accuracies for the year 2019

LULC	Vegetation	Soil	Built Up	Deep Water	Shallow Water	User Accuracy
Vegetation	97.10	5.25	2.89	1.02	0	92.04
Soil	2.72	92.24	3.57	0.81	8.19	89.24
Built Up area	0.18	3.48	93.74	0	0	91.43
Deep Water	0	0.03	0	94.10	9.31	93.37
Shallow Water	0	0	0	4.07	82.50	80.42
	100	100	100	100	100	
Producer Acc	97.81	92.22	94.76	93.23	81.34	
Overall Accuracy = 92.18						
Kappa Coefficient = 0.90						

Table 4. Confusion matrix of classification accuracies for the year 2020

LULC	Vegetation	Soil	Built Up	Deep Water	Shallow Water	User Accuracy
Vegetation	98.81	3.45	3.72	1.02	0	95.34
Soil	1.19	95.10	3.43	0	6.42	93.27
Built Up area	0	1.45	90.23	0	0	89.85
Deep Water	0	0.0	2.62	90.75	5.83	91.53
Shallow Water	0	0	0	8.23	87.75	90.18
	100	100	100	100	100	
Producer Acc	98.21	96.23	90.25	93.12	88.92	
Overall Accuracy = 90.24						
Kappa Coefficient = 0.88						

2019 and 2020 as shown in Table 5. There was a 10.18% increase in vegetation area at Loh Liang, which is the main entrance of Komodo National Park. Furthermore, there was a 41.17% increase in vegetation area at Kanawa Island, which has many resorts. There was an 18.42% increase in vegetation area at Loh Buaya, which is the future site for the construction of Komodo Geopark. Meanwhile, Pink Beach as the most renowned beach tourist item in the park has a 21.32% increase.

The entry region to Padar Island has a 60.94% increase in vegetation area. The largest rise, 69.52% occurred in the Padar Island Tracking Area, while the smallest increase of 1.43%, occurred in Loh Sebita which is the Mangrove area. From 2019 to 2020, the vegetation in Komodo National Park increased by 31.86% on average from 7 tourism spots. The results showed that the decrease in the number of tourists during Covid-19 aided in the improvement of vegetation. The island area that was not covered with vegetation in 2019 due to tourism activities such as hiking, camping, and tracking was mostly covered with

Table 5. Total Vegetation Area

Area	Vegetation Area (Pixel)		Pixel Addition	Percentage (%)
	2019	2020		
Loh Liang	1632495	1817455	184960	10.18%
Kanawa Island	503765	856375	352610	41.17%
Loh Buaya	735921	902110	166189	18.42%
Pink Beach	246732	313590	66858	21.32%
Padar Island Entrance	135035	345683	210648	60.94%
Padar Island Tracking Area	176349	578642	402293	69.52%
Loh Sebita	1019742	1034584	14842	1.43%
Average				31.86%

vegetation in 2020. This result showed a positive impact on environmental change during pandemic Covid-19. Although there could be other factors at play that may have a link as well to increase vegetation area and it is need more work to do. But according to a recent study, Covid-19 lockdowns resulted a better environment such as significant reductions in air and water pollutants (Zambrano-Monserrate et al. 2020; Chakraborty et al. 2021), noise pollution (Mandal & Pal 2020), and land cover change (Khadijat et al. 2021). Furthermore, the world's changing environmental quality has acquired a favorable shift toward sustainable environmental-friendly circumstances as a result of the imposition of a lockdown. It is also reported India's megacities positive move toward sustainable environment-friendly during the pandemic such as changes of the vegetation index. According to (Firozjaei et al. 2021), Covid-19 lockdown had an impact on the proportion and health of the vegetation. Furthermore, it positively affected plant health because of the considerable reduction in air and water pollutants.

The results showed that the environmental condition of Komodo National Park, particularly the vegetation, has improved from previous years. The study also showed the increase in the area of green areas in the Komodo National Park According to the data from Badan Pusat Statistik Manggarai Barat during 2019 – 2021 number

of precipitation, number of rainy days, and duration of sunshine in Komodo National Park there just slightly different and there is no climatic fluctuations affect. Regardless of the deadly pandemic scenario, the promoting sign gives Komodo some reason to chance for a better and more recovered environmental state.

CONCLUSION

The study aims to identify environmental changes in Komodo National Park by using a support vector machine to classify area categories. The results showed that there is a change in the vegetation area and a drop in the number of tourists due to Covid-19. The most changes in vegetation occurred in the tracking area of Padar Island. It is one of Komodo National Park's most famous tourist attractions, and it accounts for up to 69.52 %. Generally, there was a 31.86% growth in vegetation area from 7 location points that became the subject of study by comparing satellite imagery in 2019 and 2020. In the future, this research can be developed when the pandemic has been declared over by WHO by adding data in the year after 2020 to be able to clearly see the changes in LULCC. This research can also be developed by comparing other machine learning classification methods ■

REFERENCES

- Al Mamun A., Hossain M.S., Em P.P., Tahabilder A., Sultana R., & Islam M.A. (2021). Small intestine bleeding detection using color threshold and morphological operation in WCE images. *International Journal of Electrical and Computer Engineering*, 11(4), 3040-3048, DOI: 10.11591/ijece.v11i4.pp3040-3048.
- Anantrasirichai N., Biggs J., Albino F., Hill P., & Bull D. (2018). Application of Machine Learning to Classification of Volcanic Deformation in Routinely Generated InSAR Data. *Journal of Geophysical Research: Solid Earth*, 123(8), 6592-6606, DOI: 10.1029/2018JB015911.
- Ariefiandy A., Purwandana D., Azmi M., Nasu S.A., Mardani J., Ciofi C., & Jessop, T. S. (2021). Human activities associated with reduced Komodo dragon habitat use and range loss on Flores. *Biodiversity and Conservation*, 30(2), 461-479, DOI: 10.1007/s10531-020-02100-8
- BPS. (2021a). Kunjungan Wisatawan Mancanegara per bulan Menurut Kebangsaan (Kunjungan), 2021. <https://www.bps.go.id/indicator/16/1470/1/kunjungan-wisatawan-mancanegara-per-bulan-menurut-kebangsaan.html>
- BPS. (2021b). Pengunjung Taman Nasional Komodo Turun 76 persen pada 2020. <https://databoks.katadata.co.id/datapublish/2021/08/03/pengunjung-taman-nasional-komodo-turun-76-persen-pada-2020>
- Chakraborty T.C., Sarangi C., & Lee X. (2021). Reduction in human activity can enhance the urban heat island: Insights from the COVID-19 lockdown. *Environmental Research Letters*, 16(5), 1-12, DOI: 10.1088/1748-9326/abef8e
- Farda N. M. (2017). Multi-temporal Land Use Mapping of Coastal Wetlands Area using Machine Learning in Google Earth Engine. *IOP Conference Series: Earth and Environmental Science*, 98(1), 1-12, DOI: 10.1088/1755-1315/98/1/012042.
- Firozjaei M.K., Fathololomi S., Kiavarz M., Jokar J., Homaee M., & Alavipinah S.K. (2021). Modeling the impact of the COVID-19 lockdowns on urban S Surface Ecological status: A case study of Milan and Wuhan cities. *Journal of Environmental Management*, 286(January), 1-10.
- Harum P.H. (2021). Kecamatan Komodo Dalam Angka. <https://manggarai Barat kab.bps.go.id/publication/2021/09/24/6293f9e0293853e7b252d95c/kecamatan-komodo-dalam-angka-2021.html>
- Health Ministry of Indonesia (2021). SITUASI COVID-19 di Indonesia (Kumulatif). <https://www.kemkes.go.id/index.php?lg=ln02>
- Jaelani L.M. (2015). Development of a New Atmospheric Correction Algorithm for Turbid Inland Waters. *Journal of The Remote Sensing Society of Japan*, 35(3), 152-152, DOI: 10.11440/rssj.35.152.
- Kemenlu RI. (2021). Update: Indonesia Travel Restrictions. <https://kemlu.go.id/losangeles/en/news/11727/indonesia-travel-restrictions>
- Khadijat A., Anthony T., Ganiyu O., & Bolarinwa S. (2021). Forest cover change in Onigambari reserve, Ibadan, Nigeria: Application of vegetation index and Markov chain techniques. *The Egyptian Journal of Remote Sensing and Space Science*, xxxx, 1-8, DOI: 10.1016/j.ejrs.2021.08.004.
- Komodo National Park (2017). Komodo National Park. <http://www.komodonationalpark.org/>
- Lee, S., Lee, K., & Kim, B. (2018). Binary Image Based Fast DoG Filter Using Zero-Dimensional Convolution and State Machine LUTs. 5(2), 131-138.
- López-Serrano P.M., López-Sánchez C.A., Álvarez-González J.G., & García-Gutiérrez J. (2016). A Comparison of Machine Learning Techniques Applied to Landsat-5 TM Spectral Data for Biomass Estimation. *Canadian Journal of Remote Sensing*, 42(6), 690-705, DOI: 10.1080/07038992.2016.1217485.
- Majumdar S. (2020). Assessment and detection of land cover changes in the southern fringe of Kolkata using remotely sensed data. *Geography, Environment, Sustainability*, 13(4), 121-132, DOI: 10.24057/2071-9388-2020-65.
- Makwinja R., Kaunda E., Mengistou S., & Alamirew T. (2021). Impact of land use/land cover dynamics on ecosystem service value—a case from Lake Malombe, Southern Malawi. *Environmental Monitoring and Assessment*, 193(8), 1-23, DOI: 10.1007/s10661-021-09241-5.
- Mandal I., & Pal S. (2020). COVID-19 pandemic persuaded lockdown effects on environment over stone quarrying and crushing areas. *Science of The Total Environment*, 732, 1-10, DOI: 10.1016/j.scitotenv.2020.139281.
- Medina A.F. (2021). What are Indonesia's Latest Guidelines on International Travel? Asean Briefing. <https://www.aseanbriefing.com/news/what-are-indonesias-latest-guidelines-on-international-travel/>

- Mishra P.K., Rai A., & Rai S.C. (2020). Land use and land cover change detection using geospatial techniques in the Sikkim Himalaya, India. *Egyptian Journal of Remote Sensing and Space Science*, 23(2), 133-143, DOI: 10.1016/j.ejrs.2019.02.001.
- Naiemi F., Ghods V., & Khalesi H. (2021). A novel pipeline framework for multi oriented scene text image detection and recognition. *Expert Systems with Applications*, 170(November 2020), 1-16, DOI: 10.1016/j.eswa.2020.114549.
- Otsu N. (1979). A Threshold Selection Method from Gray-Level Histograms. *IEEE Transaction on Systems, Man and Cybernetics*, 20(1), 62-66.
- Patel S.K., Verma P., & Shankar Singh G. (2019). Agricultural growth and land use land cover change in peri-urban India. *Environmental Monitoring and Assessment*, 191(9), 1-17, DOI: 10.1007/s10661-019-7736-1.
- Pelletier C., Valero S., Inglada J., Champion N., Sicre C.M., & Dedieu G. (2017). Effect of training class label noise on classification performances for land cover mapping with satellite image time series. *Remote Sensing*, 9(2), 1-24, DOI: 10.3390/rs9020173.
- Putra D. (2010). *Pengolahan Citra Digital* (Westriningsih (ed.)). Penerbit Andi.
- Rao B.S. (2020). Dynamic Histogram Equalization for contrast enhancement for digital images. *Applied Soft Computing Journal*, 89, 106-114, DOI: 10.1016/j.asoc.2020.106114.
- Saputra R.A. (2021). Comparison of wavelet transform for image recognition system using Learning Vector Quantization. *SemanTIK*, 7(1), 1-8, DOI: 10.5281/zenodo.5034914.
- Shih H., Stow D.A., & Tsai Y.H. (2019). Mapping, Guidance on and comparison of machine learning classifiers for Landsat-based land cover and land use. *International Journal of Remote Sensing*, 40(4), 1-15, DOI: 10.1080/01431161.2018.1524179.
- Talukdar S., Singha P., Mahato S., Shahfahad Pal S., Liou Y. A., & Rahman A. (2020). Land-use land-cover classification by machine learning classifiers for satellite observations-A review. *Remote Sensing*, 12(7), 1-24, DOI: 10.3390/rs12071135.
- Thome K., Markham B., Barker J., Slater P., & Biggar S. (1997). Radiometric calibration of Landsat. *Photogrammetric Engineering and Remote Sensing*, 63(7), 853-858.
- UNESCO. (2020). Komodo National Park. <https://whc.unesco.org/en/list/609/>
- Verma P., Singh R., Singh P., & Raghubanshi A.S. (2020). Urban ecology – current state of research and concepts. *Urban Ecology*, 3-16, DOI: 10.1016/b978-0-12-820730-7.00001-x.
- Veyadi Purba J.H., Fathiah R., & Steven (2021). The Impact of COVID-19 on the Tourism Sector in Indonesia. *Riset : Jurnal Aplikasi Ekonomi*, 3(1), 389-401.
- Voronin V. (2019). Modified Local and Global Contrast Enhancement Algorithm for Color Satellite Image. *EPJ Web of Conferences*, 224, 1-5, DOI: 10.1051/epjconf/201922404010.
- Wang L., Weng L., Xia M., Liu J., & Lin H. (2021). Multi-resolution supervision network with an adaptive weighted loss for desert segmentation. *Remote Sensing*, 13(11), 1-18, DOI: 10.3390/rs13112054.
- WHO (2021). Coronavirus disease (COVID-19) pandemic. <https://www.who.int/emergencies/diseases/novel-coronavirus-2019>
- Worldometers (2021). COVID-19 CORONAVIRUS PANDEMIC. <https://www.worldometers.info/coronavirus/>
- Wu C.F., Deng J.S., Wang K., Ma L.G., & Tahmassebi A.R.S. (2016). Object-based classification approach for greenhouse mapping using Landsat-8 imagery. *International Journal of Agricultural and Biological Engineering*, 9(1), 79-88, DOI: 10.3965/ijjabe.20160901.1414.
- Wu X., Liu X., Hiramatsu K., & Kashino K. (2017). CONTRAST-ACCUMULATED HISTOGRAM EQUALIZATION FOR IMAGE ENHANCEMENT. *typically* 256, 3190-3194.
- www.komodonationalpark.org. (n.d.). Zoning Komodo National Park. www.komodonationalpark.org
- Yuniar E. (2018). Validasi Produk Reflektan Permukaan Landsat-8 Menggunakan Data In-Situ (Studi Kasus : Danau Kasumigaura, Jepang).
- Zambrano-Monserrate M.A., Ruano M.A., & Sanchez-Alcalde L. (2020). Indirect effects of COVID-19 on the environment. *Science of The Total Environment*, 728, 1-4, DOI: 10.1016/j.scitotenv.2020.138813.